Burst propagation in Texas Helimak

2016 Plasma Phys. Control. Fusion 58 054007

(http://iopscience.iop.org/0741-3335/58/5/054007)

IOP Publishing Plasma Physics and Controlled Fusion

Plasma Phys. Control. Fusion **58** (2016) 054007 (8pp) doi:10.1088/0741-3335/58/5/054007

Burst propagation in Texas Helimak

F A C Pereira[1], D L Toufen[1,2], Z O Guimarães-Filho[1], I L Caldas[1] and K W Gentle[3]

[1] Institute of Physics, University of São Paulo, 05508-090 São Paulo, São Paulo, Brazil
[2] Federal Institute of Education, Science and Technology of São Paulo–IFSP, 07115-000 Guarulhos, São Paulo, Brazil
[3] Department of Physics and Institute for Fusion Studies, The University of Texas at Austin, Austin, Texas 78712, USA

E-mail: faugusto@if.usp.br

Received 30 September 2015, revised 21 January 2016
Accepted for publication 27 January 2016
Published 19 April 2016

Abstract

We present investigations of extreme events (bursts) propagating in the Texas Helimak, a toroidal plasma device in which the radial electric field can be changed by application of bias. In the experiments analyzed, a large grid of Langmuir probes measuring ion saturation current fluctuations is used to study the burst propagation and its dependence on the applied bias voltage. We confirm previous results reported on the turbulence intermittency in the Texas Helimak, extending them to a larger radial interval with a density ranging from a uniform decay to an almost uniform value. For our analysis, we introduce an improved procedure, based on a multiprobe bidimensional conditional averaging method, to assure precise determination of burst statistical properties and their spatial profiles. We verify that intermittent bursts have properties that vary in the radial direction. The number of bursts depends on the radial position and on the applied bias voltage. On the other hand, the burst characteristic time and size do not depend on the applied bias voltage. The bias voltage modifies the vertical and radial burst velocity profiles differently. The burst velocity is smaller than the turbulence phase velocity in almost all the analyzed region.

Keywords: plasma turbulence, plasma intermittence, Helimak

(Some figures may appear in colour only in the online journal)

1. Introduction

Plasma edge electrostatic turbulence affects magnetically confined plasmas in tokamaks, stellarators, and reversed field pinches and has characteristics that are common to all of these devices [1–4]. Generally, such observed turbulence consists of two components: a broadband background fluctuation and a sequence of large intermittent bursts [5, 6]. These bursts contribute significantly to the particle transport observed in the edge and the scrape-off layer (SOL) of tokamaks, stellarators, and reversed field pinches, and also in other magnetized devices [3, 5–14]. In some experimental observations the burst origin has been attributed to macroscopic instabilities [15] or identified with random processes [16, 17]. Although other investigations in fusion devices have revealed additional relevant properties of these bursts, the need for better understanding of the basic properties and nature of such extreme events remains. In this context, bursty turbulence similar to that observed at the plasma edge in fusion devices has also been investigated in other magnetic plasma devices [4, 7–11, 18–21].

On the other hand, several procedures have been tried to control plasma turbulence at the plasma edge and to improve the confinement in fusion devices, for instance by injecting radio frequency (RF) waves at the plasma edge [22, 23] or by imposing an external electric potential that changes the radial electric field profile [24–26]. Experiments have also been performed to study electrostatic turbulence and bursts in plasmas with flow and magnetic shear in Helimaks [27–31]. The Helimak is one of a class of basic plasma experiments with characteristics of fusion plasmas in a simple geometry. This basic plasma toroidal device is a sheared cylindrical slab [27], that simplifies the turbulence description and provides results that can be used to understand the plasma edge and the SOL in major fusion machines [28, 32, 33].

One of these devices, the Texas Helimak, is a simplified model system for the study of drift-wave plasma turbulence. It approximates an infinite cylinder, the sheared cylindrical slab, with an MHD equilibrium that depends on a single, radial variable [27]. The magnetic field lines are helices of variable pitch. Although the experiment is finite, the open helical field lines are sufficiently long to be effectively infinite.

Control of turbulence by biasing has been investigated in the Texas Helimak [27, 34], which is specially configured to allow varying the radial electric field with bias. Bias is applied using a set of electrically isolated horizontal metal plates at the top and at the bottom of the vacuum chamber, nearly perpendicular to the magnetic field. For negative biasing, turbulence control has been investigated and states of greatly reduced turbulence have been achieved [27, 34]. However, despite the alteration of the flow shear by the applied bias voltage, no turbulence dependence on the flow shear has been identified [34]. Furthermore, evidence was found that turbulent transport in this device is strongly affected by wave particle resonances and by a kind of shearless transport barrier [35]. On the other hand, for positive biasing, turbulence shows enhanced broadband spectra and non-Gaussian probability distribution functions (PDFs) with extreme events associated with bursts [36]. Recently, it was reported that the occurrence of bursts and their propagation, in a specific plasma region with roughly uniform equilibrium density gradient, varies with changes in the radial electric field profile [37].

In this work, we confirm previous results reported on the Texas Helimak concerning turbulence intermittency, extending them for a larger radial range and improving the procedure to analyze the burst identification and propagation. Thus, for new Texas Helimak discharges with positive biasing, we analyze ion saturation current fluctuations obtained by a large set of Langmuir probes. The data were collected in a large radial range, containing a region with an almost uniform density gradient, as in the tokamak plasma edge, and another with a uniform density, as in the tokamak SOL.

We introduce a new procedure to improve burst selection and assure a more precise determination of burst properties, spatial profiles, and velocities. Namely, we apply a conditional average to a set of neighboring probes with some of them as references to detect bursts. We verify that intermittent bursts have different properties along the radial direction. The number of bursts depends on the radial position and on the applied bias voltage. On the other hand, the burst characteristic time and size do not depend on the applied bias voltage. The bias voltage modifies the vertical and radial burst velocity profiles differently. We distinguish the burst velocities from the turbulence phase velocity, finding that these velocities are approximately equal only in a specific radial region, as previously reported [37]. Outside this region, the burst velocity is smaller than the turbulence phase velocity.

In section 2, we review the experimental set-up. In section 3, we describe the procedure to identify the bursts in the Texas Helimak. Finally, in section 4 we present the obtained burst properties and velocity radial profiles and their dependence on the positive bias voltage.

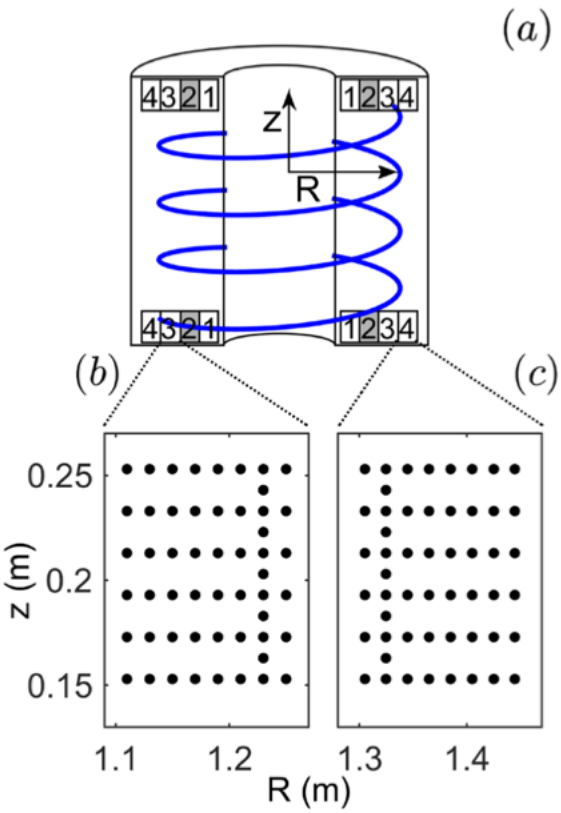

Figure 1. (a) Texas Helimak vacuum chamber showing a sample of the magnetic field lines, the plates used as a support for the Langmuir probes, and the plates, in gray, where the external voltage is applied. (b), (c) Two Langmuir probe distributions used in the discharges considered in this work.

2. Experimental set-up

The experiments reported in this work were performed at Texas Helimak [27], located at the University of Texas at Austin. Texas Helimak is a toroidal machine mainly devoted to basic plasma turbulence study. The magnetic field is produced by a combination of a toroidal and a vertical set of coils producing helical magnetic field lines with curvature and shear as shown in figure 1(a). Because of these properties, the Helimak geometry can be well described by the sheared cylindrical slab since the connection lengths are long enough to neglect end effects. In the analyzed experiments, the toroidal field is about 0.1 T, which is combined with the weaker vertical field creating helical magnetic field lines with a connection length of several meters (about 40 m at the middle of the machine, $R = 1.1$ m).

The Texas Helimak has a vacuum vessel with rectangular cross section of internal and external radii 0.6 m and 1.6 m, respectively, and 0.6 and 2 m height. For the experiments presented in this work the gas is argon at 1.3 mPa and it was heated by a microwave source with 6 kW of power at 2.4 GHz coupled through a window located on the high field side. On the top and bottom of the machine there are four sets of metallic plates where the magnetic field lines start and terminate. These plates are used as a support for the Langmuir probes and to apply external electric potentials (bias) to change the radial electric field profile. The shot duration is up to 20 s and

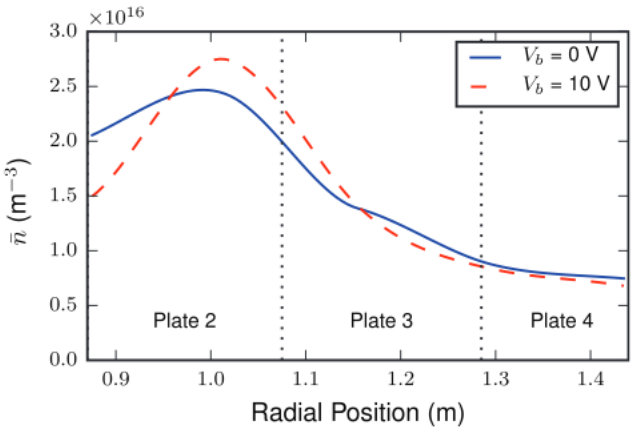

Figure 2. Equilibrium density radial profiles for grounded (solid line) and +10 V (dashed line) of imposed bias values. The bars indicate the plates where the bias voltage is applied.

the plasma is in an almost steady state with stationary conditions for 10 s, the time interval considered for the fluctuation analysis described in this work. The diagnostic system counts more than 700 Langmuir probes mounted on the four sets of bias plates. The data were taken by two digitizers, one with 96 channels and 500 kHz sample rate for turbulence measurements, and another one with 128 channels and 7 kHz sample rate for equilibrium measurements. In this work we analyze the ion saturation current fluctuations on the low field side, using two different probe distributions (figures 1(b) and (c)). These two probe distributions are located at plates 3 and 4. Through these two distributions, we study the turbulence and plasma structure characteristics as we move further from the density maximum (usually on plates 1 and 2) and the bias imposing plate (plate 2). These probe distributions have grids of probes measuring ion saturation current, which allow us to make a spatial characterization of the turbulence and of the plasma structures. The study of this wide range of radial positions has a special value for understanding the turbulent particle transport in tokamaks, since different positions on the Texas Helimak can be related to different plasma regions of a tokamak. Figure 2 shows the equilibrium density radial profile for two different bias values. This figure shows that the Helimak plasma at 1.11 m < R < 1.25 m (plate 3 region) has a significant radial gradient, like the tokamak plasma edge. On the other hand, the Helimak plasma at $R > 1.3$ m (plate 4 region) has an almost uniform density profile, like the tokamak SOL.

3. Burst identification

As also observed in other experimental turbulence investigations, in the Texas Helimak, turbulent signals have two components: the almost stationary nearly Gaussian random fluctuations and the intermittent bursts [34]. The turbulence in this device is highly dependent on the radial position and the external bias values [36].

In figure 3(a), we present a short time interval of the saturation current signal, measured by a Langmuir probe at $R = 1.365$ m and $Z = 0.233$ m in a discharge with +10 V of

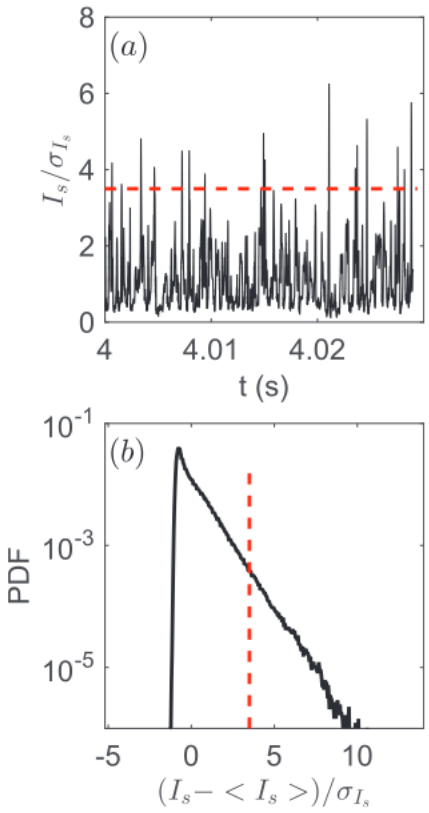

Figure 3. Example of (a) an ion saturation current signal with the threshold used to select bursts indicated by a dashed line and (b) the PDF of the relative fluctuation, $(I_s - \langle I_s \rangle)/\sigma_{I_s}$, the dashed line indicates the threshold used to select bursts in the long PDF tail at the positive side. The ion saturation current was measured at the position $R = 1.365$ m and $Z = 0.233$ m in a discharge with bias $V_b = +10$ V.

imposed bias. In figure 3(a), we observe that the time series clearly presents many bursts (spikes), with peaks several standard deviations above the mean value. The red dashed line marks a 3.5 standard deviation threshold used in this work as a criterion to define whether a peak in the time series is a burst. The presence of bursts with such high frequency of occurrence changes the PDF of the entire time series [38, 39]. The PDF of the relative ion saturation fluctuation, $(I_s - \langle I_s \rangle)/\sigma_{I_s}$, for the Langmuir probe for the same condition is shown in figure 3(b) in a solid black line. The observed PDF clearly has a long tail on the positive side due to the presence of the bursts. In figure 3(b), the red dashed line indicates the 3.5 standard deviation threshold used to define the part of the PDF tail that was used to consider a peak as a burst. We can see the part of this tail considered in the burst analysis by a high threshold choice. This high threshold value is used to minimize, in our conditional analyses, the chance of including common oscillations in the signal as bursts.

In the Texas Helimak it was previously observed that the burst rate can be substantially modified by changing the value of an externally imposed bias [37]. Once the presence of extreme events changes the ion saturation current PDF, the third and fourth normalized statistical moments, skewness and kurtosis respectively, can be used as an indication of the burst contribution. Following this idea, figure 4 shows skewness (a)

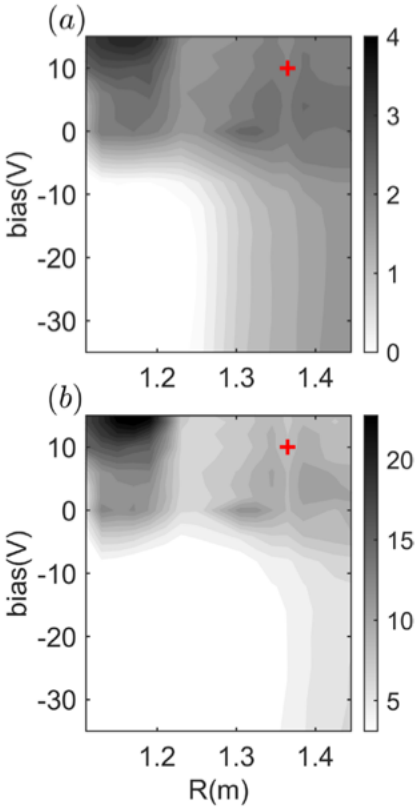

Figure 4. Ion saturation current skewness (a) and kurtosis (b) as a function of the radial position and the bias of the discharge for a fixed vertical position, $Z = 0.233$ m. The cross indicates the radial position considered in the signals shown in figure 3.

and kurtosis (b) as a function of the radial position and the external imposed bias values. In these figures, darker regions mark higher values of skewness or kurtosis, which indicates an increase in the presence of extreme events. Observing figures 4(a) and (b) it is clear that bias changes the turbulence regime, enhancing the skewness and kurtosis for positive bias and reducing both for negative bias. At the larger radii, the bias effects are reduced since the bias is applied at an inner radial region, $0.863 \text{ m} < R < 1.075$ m, but even for $R > 1.4$ m the bias effect can be observed in skewness and kurtosis.

Observing the statistical moments presented in figure 4 one can infer the extensive number of extreme events in the Helimak turbulence, especially for positive bias values, since the values of the kurtosis and skewness are higher when positive bias values are imposed. Thus, as a consequence of the results shown in figure 4, we will focus our extreme event analysis on positive bias values. In order to study a wide range of radial positions, we analyze data from two different probe sets located on plates 3 and 4, shown in figures 1(b) and (c) respectively.

In order to evaluate the burst rate, we count the number of bursts in the ion saturation current signals. Figure 5 shows the burst rate as function of the radial position for four different bias values. Figure 5 shows the burst rate in the density gradient region (up to $R \approx 1.25$ m), changing from approximately 200 bursts per second for $V_b = 0$ V (grounded plates) to around 500 bursts per second for $V_b = 14$ V. For larger radial positions, the imposed bias has almost no effect on the

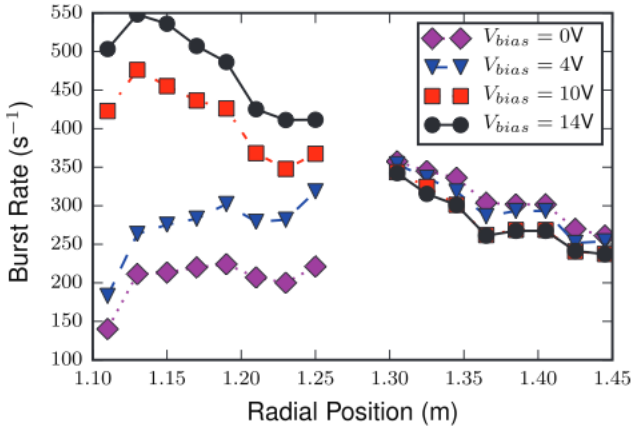

Figure 5. Burst rate as a function of the radial position for several bias values and $z = 0.253$ m. Notice that for inner radial positions, $R < 1.30$ m, the bias values increase the burst rate; on the other hand, for external positions the bias effect on the burst rate is negligible.

burst rate. This suggests that the bursts do not propagate far in the radial direction, as the increase in the number of bursts in one radial region has no effect on the number of bursts in the other. Considering the results shown in figures 4 and 5, we can confirm that the burst presence on the signal generates a heavy-tail distribution that can be observed by measuring the skewness and especially the kurtosis of the data series.

Using our criterion for burst selection, we performed a conditional analysis on the time series to study the mean properties of the bursts. The conditional analysis consists of using the time when each burst is detected at a defined reference probe as a new time reference for performing averages [6]. Using this technique it is possible to calculate the mean temporal profile of the bursts. Figure 6 shows this mean temporal profile of the bursts as a solid black line for a reference probe located at $R = 1.21$ m (and $Z = 0.233$ m) for a discharge with $V_b = +10$ V. From the temporal burst profile we cannot observe a valley of density right before (or after) the border of the burst. This suggests that the bursts are not created close to the measurement region by a local inhomogeneous redistribution of density. The time profiles show a clear symmetry between the right- and the left-hand borders.

Additionally, the conditional analysis allows us to infer information about the propagation of the bursts along the probe grid. For this, we use the time reference of each burst located at the reference probe to compute the average shape of the time series at the neighboring probes. The results of these multiprobe conditional analyses are shown in figure 6(a) for three probes at the same vertical position and in figure 6(b) for three probes at the same radial position, in both cases using the same reference probe. The time delay between the detections of a burst when considering neighboring probes is clearly related to the mean propagation of the bursts across the probe grid. However, as will be shown in the following, only considering the delay between probes in a given direction is not enough. A simple example to illustrate this problem is the detection of plane wave velocity. When we use time delays of the maxima between pairs of points in order to estimate the velocity components, the velocity obtained will always

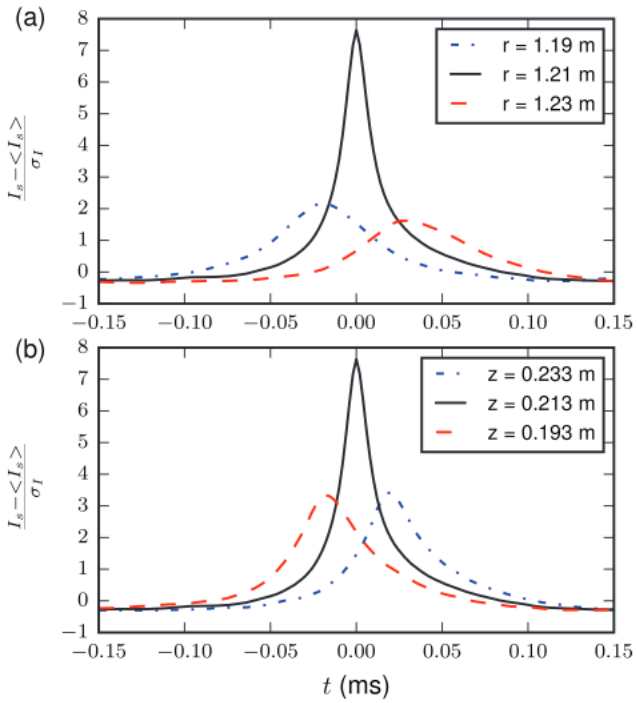

Figure 6. Conditional average profile of a burst at a reference probe, solid black line, and the corresponding conditional average on two neighboring probes in (a) radial direction and (b) vertical direction. In this figure, the delay between the conditional averages is a clear evidence of the propagation of the bursts across the grid of probes.

be higher than the real (total) velocity of the structure when the propagation velocity is not aligned with the difference between positions of the two probe. In this case, an analysis that takes into account the spatial structure is required.

4. Burst spatial and propagation characteristics

For a reliable analysis of the burst propagation and properties, we need to make sure that we make unbiased estimates of the structure profile. The one-probe burst selection algorithm, while reliable for single-probe analysis, may lead to a wrong structure spatial profile, as the structure determination relies on data from several probes and this method mixes bursts that are not centered on the selected reference probe. If we take into account non-centered structures in the conditional analysis calculations, we get blurred structures: the off-center structures will increase the value of the conditional average of the neighboring probes (because some structure centers pass through them) and decrease the average of the reference probe.

We impose a new condition on the burst selection algorithm to guarantee that the structures are centralized on the reference probe: we look at the turbulence signal of the neighbor probes for bursts. If a neighbor probe has a more intense burst (in standard deviations above the mean value) than the reference probe, we discard this burst, as we consider that it is not centered on the reference probe. An example of the conditional averages of the probe grid is shown in figure 7(a), for $t = 0$ (burst occurring on the reference probe). Figure 7(b)

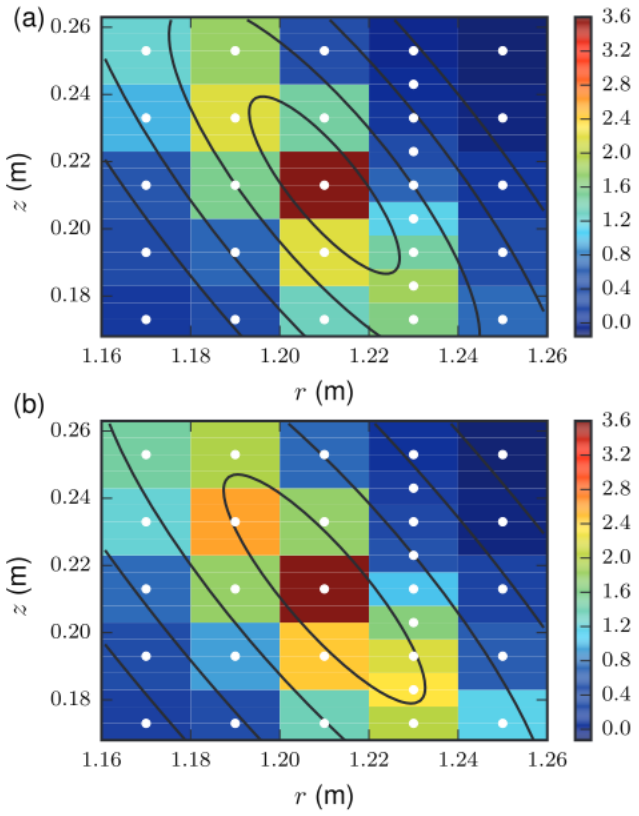

Figure 7. The conditional average of the saturation current for each probe (plotted as dots) in the grid is shown in a color scale using (a) only bursts centered on the reference probe and (b) all bursts identified on the reference probe. The solid lines represent the level sets of the fitted bidimensional model. The difference between (a) and (b) makes clear the improvement of the burst localization when information from neighboring probes is taken into account.

shows the conditional averages when we do not enforce the centralization condition, resulting in blurred bursts, that are spatially broader and have a lower maximum. In spite of the changes to the detected burst spatial structure, this new selection algorithm does not much affect the estimated burst velocities. Figure 7 also highlights some characteristics of the burst structure: it is a tilted structure with two characteristic lengths, the shorter one that is approximately aligned with the line $R = Z$, less than 2 cm in length; and the longer one perpendicular to it, about 4 cm in length.

We used these spatial profiles to develop a phenomenological structure shape model [37]. In this model, the burst structure is described by two perpendicular characteristic lengths and has a lorentzian profile. For the propagation part; we suppose that the structure has a constant velocity and is located at the reference probe at $t = 0$. The fitting function is

$$I_s(R,Z,t) = I_f + I_b(t)\left\{1 + \left[\frac{(R - R_0(t))\cos\theta + (Z - Z_0(t))\sin\theta}{s_1(t)}\right]^2 + \left[\frac{(Z - Z_0(t))\cos\theta - (R - R_0(t))\sin\theta}{s_2(t)}\right]^2\right\}^{-1},$$

where $s_1(t)$ and $s_2(t)$ are the two characteristic lengths (with $s_1 > s_2$); θ is the structure tilt angle; $(R_0(t), Z_0(t))$ is the structure

center position, that, in this case, is $(R_{ref} + v_r t, Z_{ref} + v_z t)$. $I_b(t)$ is the amplitude of the burst peak at time t. For the time dependence of the burst amplitude and characteristic lengths, we considered that the burst amplitude decays exponentially with time; and the structure suffers a diffusion (an increase of the characteristic lengths for $|t| > 0$) conserving the ratio $\lambda = s_2/s_1$. So, we can write

$$I_b(t) = I_0 e^{-\frac{|t|}{\tau}}, \qquad s_1(t) = \sqrt{s_0^2 + \delta|t|}.$$

We estimate the function parameters using a non-linear least squares fit. For this fit, we use a square neighborhood with sides of 8 cm, centered on the reference probe, for a time interval of 60 μs centered on $t = 0$. The result of a fitting can be seen as black contour plots in figure 7. We estimate the burst structure characteristics for many radial positions by changing the reference probe, keeping the restriction that we need at least one row of probes in each radial direction. We choose the reference probes at a vertical position $Z = 0.213$ m. We also use shots with different values of imposed bias to see how bias affects the burst propagation characteristics. We conclude that the dependence of all the burst parameters on the imposed bias is weak for the bursts located in the almost constant density region (plate 4). It is interesting to note that the burst rate in this region also does not depend on the bias value (see figure 5). The background parameter is always small ($|\Gamma| < 0.2$); this result agrees with examination of the conditional average temporal profiles from figure 6. The small negative value is probably because of the weight that the burst structures have on the average value of Γ_t, as the difference between the mean and the median is about $0.3\sigma_\Gamma$. We use the mid-height area, $S = \pi s_1 s_2$, at $t = 0$ as a measure of the burst size, because it is related to the excess plasma contained in this structure. Figure 8(a) shows the burst size as a function of the radius for four different bias values. The burst size seems not to change much with the bias, but the structures get bigger when we go further on the low-field side: the structures at $R = 1.385$ m are about ten times bigger than those at $R = 1.13$ m. Another important feature that we obtain from the fittings is the burst characteristic time τ, that is related to the mean burst duration as it is the time that the density maximum takes to drop to 1/e of its maximum value ($t = 0$). Figure 8(b) shows the burst characteristic time as a function of the same radial positions and bias values. We can see that it follows the trend observed for the burst size: the bursts survive longer further from the plasma center. When we look at figures 8(a) and (b) together, we can see that the imposed bias has little effect on both burst properties, even close to the bias plates. So, while the bias has an important effect on the burst suppression and abundance, it does not change the radial profiles of the burst characteristic time and size.

The fitted vertical and radial velocities are presented in figure 9. From figure 9(a) we can see two different behaviors: near the bias plate in the uniform density gradient region the radial velocity does not change much with R, but increases with the bias, while at larger radii (uniform density region) it grows to 500 m s^{-1}. This result, together with the burst duration and size (figure 8), suggests that these structures are

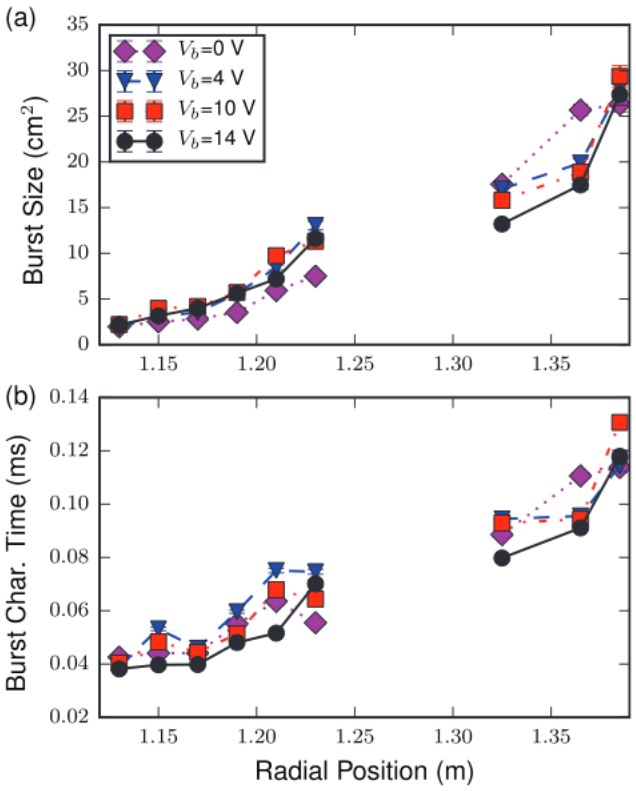

Figure 8. Burst characteristics as a function of the radial position estimated using the bidimensional fit. (a) The burst size (the fitted half height area of the density distribution at $t = 0$). (b) The burst characteristic time, which is the time that the maximum of the density distribution takes to decay to e^{-1} of its value at $t = 0$.

important to the turbulent radial transport. For the vertical velocity, presented in figure 9(b), we have a different radial profile: the velocity seems to grow from $R = 1.13$ m to a maximum somewhere around $R = 1.20$ m and decreases from $R = 1.32$ m until it reaches negative values at $R = 1.38$ m. The effect of bias on the vertical velocity is clear: the vertical propagation of the structures is strongly affected by the bias near the bias plate, increasing the vertical velocity as we increase the bias. The bias effect on the vertical velocity diminishes as we move further from the plate, until it is no longer observed for $R > 1.30$ m.

In the Texas Helimak, it was observed that the burst velocities are approximately equal to the overall turbulence phase velocity for a specific region near the bias plates [37]. To verify if this relation holds for a large range of radial positions investigated in this article, we estimated the average overall turbulence phase velocity using the $S(k, f)$ histogram [37, 40]. The estimated phase velocities are presented in figure 10. From this figure, we can see that both radial and vertical phase velocity depend strongly on the imposed bias in the region near the bias plate ($R < 1.3$ m), and that the velocities increase as we increase the imposed bias. On the other hand, the bias effect is not observed at larger radii ($R > 1.3$ m). The radial dependence near the bias plate is about the same for both vertical and radial phase velocities: both increase between $R = 1.13$ m and $R = 1.23$ m. However, while the radial phase velocity assumes a constant value from $R = 1.3$ m, the vertical phase velocity decreases slowly in this region.

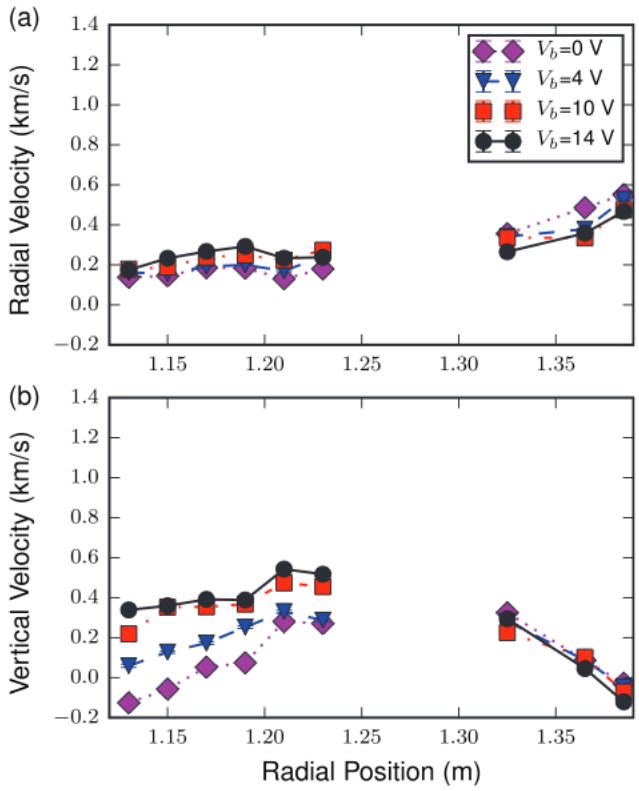

Figure 9. Burst velocity radial profiles in (a) radial direction and (b) vertical direction for several bias values.

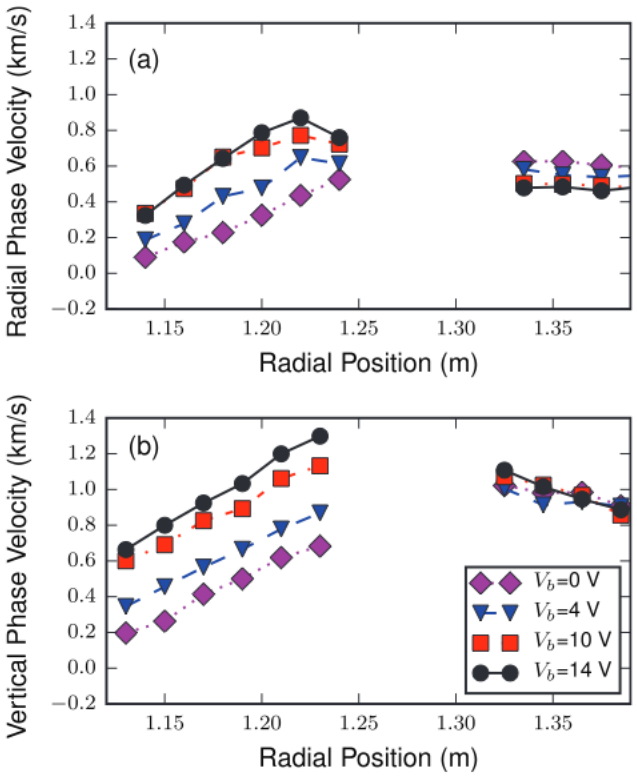

Figure 10. Turbulence average phase velocity radial profile in (a) radial direction and (b) vertical direction for the same bias values as in figure 9.

A comparison of figures 9(a) and 10(a) suggests that the burst propagation in the radial direction has a different behavior from the wave propagation of the overall turbulence, as their dependences on bias and on the radial position are not the same. While the burst radial velocity is weakly affected by the bias and increases at larger radii, the change in the bias values can double the radial phase velocity in the uniform gradient region. In the uniform density region, radial burst velocities and radial wave phase velocities have the same weak dependence on the bias, but the burst velocities increase with radius while the phase velocity does not. In the vertical direction (figures 9(b) and 10(b)), the effect of the bias is the same for both burst and phase velocities: it increases the velocity near the bias plate and has no effect far from it.

Taking into account previously measured values of $\vec{\mathbf{E}} \times \vec{\mathbf{B}}$ drift velocities in the Texas Helimak, which vary from 0.5 to 1.0 km s^{-1}, the burst velocities and specially the phase velocities are of the same order as the expected $\vec{\mathbf{E}} \times \vec{\mathbf{B}}$ drift velocities. From this similarity and based on the consistent change of the phase velocities with the applied bias voltage, it is possible to assume that the phase velocities are directly related to the $\vec{\mathbf{E}} \times \vec{\mathbf{B}}$ drift velocity. On the other hand, vertical and principally radial burst velocities are lower than phase velocities or even than other plasma velocity values such as the ion sound velocity, which is of the order of 10 km s^{-1}. Furthermore, the low temperature ion diamagnetic drift, as well as the magnetic gradient and curvature drifts, are negligible [34]. In addition, the vertical plasma flow velocity, obtained through the spectroscopic measurements [34], has a similarity to the phase velocities measured by probes, so it is possible to infer a major influence of the plasma flow velocity on the measured phase velocities.

5. Conclusions

We used data from new experiments performed in the Texas Helimak to analyze turbulent ion saturation current fluctuations in a large radial range, from an inner region with an almost uniform density gradient to an outer region with almost uniform density. Thus, the same Texas Helimak configurations allowed us to identify different intermittent burst regimes at different radial positions. The plasma profiles and turbulence analyzed are similar to those observed in the tokamak plasma edge, where a density gradient exists, and in the tokamak SOL, where the density is approximately uniform. In fact, the fluctuations analyzed in this article are most similar to the tokamak SOL due to the reported high relative fluctuations and burst frequency.

To determine precisely how the bursty intermittence changes with the applied bias voltage and with the radial position, we introduce a procedure to identify high amplitude bursts and to follow their propagation in the plasma. Thus, we only considered bursts with spatial structures observed in a set of neighboring probes, with the maximum located at the reference probe. This procedure showed that the burst size considering only one reference probe was overestimated. This procedure allows us to improve the burst selection and assure precise determination of burst properties and their spatial profiles. Furthermore, the procedure used allows an accurate

determination of the burst propagation velocity. In fact, we could distinguish the radial profiles of the burst and phase velocities, observing that they are usually different.

Changes in burst rate in the radial direction, as well as the measured values of their radial velocity and characteristic time, indicate that individual bursts are hardly propagating long enough to cover the whole analyzed radial interval. Further investigations should be done to confirm this statement.

Finally, this burst analysis may contribute to understanding the role of bursts in local radial particle transport in magnetically confined plasmas.

Acknowledgments

We would like to thank the Brazilian agencies FAPESP (processes 2012/22108-5, 2011/19296-1 and 2014/07043-0), CNPq (processes 470380/2012-8 and 300632/2010-0), and CAPES for financial support of this work.

References

[1] Hidalgo C 1995 *Plasma Phys. Control. Fusion* 37 A53
[2] Gentle K W 1995 *Rev. Mod. Phys.* 67 809
[3] Zweben S J, Boedo J A, Grulke O, Hidalgo C, LaBombard B, Maqueda R J, Scarin P and Terry J L 2007 *Plasma Phys. Control. Fusion* 49 S1–23
[4] Horton W 1999 *Rev. Mod. Phys.* 71 735
[5] Sánches R *et al* 2000 *Phys. Plasmas* 7 1408
[6] Antar G Y, Devynck P, Garbet X and Luckhardt S C 2001 *Phys. Plasmas* 8 1612
[7] Antoni V, Carbone V, Martines E, Regnoli G, Serianni G, Vianello N and Veltri P 2001 *Europhys. Lett.* 54 51
[8] Baptista M S, Caldas I L, Heller M V A P and Ferreira A A 2003 *Phys. Plasmas* 10 1283
[9] Boedo J A *et al* 2001 *Phys. Plasmas* 8 4826
[10] Xu Y H, Jachmich S, Weynants R R and the TEXTOR team 2005 *Plasma Phys. Control. Fusion* 47 1841
[11] Carter T A 2006 *Phys. Plasmas* 13 010701
[12] Antar G Y, Krashennikov S I, Devynck P, Doerner R P, Hollmann E M, Boedo J A, Luckhardt S C and Conn R W 2001 *Phys. Rev. Lett.* 87 065001
[13] Barni R and Riccardi C 2014 *Plasma Phys. Control. Fusion* 51 085010
[14] Fedorczak N *et al* 2012 *Phys. Plasmas* 19 072314
[15] Furno I *et al* 2008 *Phys. Rev. Lett.* 100 055004
[16] Garcia E G 2012 *Phys. Rev. Lett.* 108 265001
[17] Garcia O E, Fritzner S M, Kube R, Cziegler I, LaBombard B and Terry J L 2013 *Phys. Plasmas* 20 055901
[18] Farge M, Schneider K and Devynck P 2006 *Phys. Plasmas* 13 042304
[19] Vannucci A, Nascimento I C and Caldas I L 1989 *Plasma Phys. Control. Fusion* 31 147
[20] Windisch T *et al* 2011 *Plasma Phys. Control. Fusion* 53 085001
[21] Spolaore M *et al* 2002 *Phys. Plasmas* 9 4110
[22] Ferreira A A, Heller M V A P, Caldas I L, Lerche E A, Ruchko L F and Baccalá L A 2004 *Plasma Phys. Control. Fusion* 46 669
[23] Uckan T, Richards B, Bengtson R D, Carreras B A, Guoxiang Li, Hurwitz P D, Rowan W L, Tsui H Y W and Wootton A J 1995 *Nucl. Fusion* 35 487
[24] Hidalgo C *et al* 2005 *Nucl. Fusion* 45 S266
[25] Van Oost G *et al* 2003 *Plasma Phys. Control. Fusion* 45 621
[26] Nascimento I C *et al* 2005 *Nucl. Fusion* 45 796
[27] Gentle K W and He H 2008 *Plasma Sci. Technol.* 10 284
[28] Rypdal K and Ratynskaia S 2005 *Phys. Rev. Lett.* 94 225002
[29] Ricci P, Rogers B N and Brunner S 2008 *Phys. Rev. Lett.* 100 225002
[30] Miller S H, Fasoli A, Labit B, McGrath M, Pisaturo O, Plyushchev G, Podesta M and Poli F M 2005 *Phys. Plasmas* 12 090906
[31] Øynes, F J, Olsen O M, Pecseli H L, Fredriksen A and Rypdal K 1998 *Phys. Rev.* E 57 2242
[32] Luckhardt S 1999 The Helimak: a one dimensional toroidal plasma system *Technical Report* No. UCSD-ENG-069, University of California, San Diego (http://orion.ph.utexas.edu/starpower)
[33] Perez J C, Horton W, Gentle K W, Rowan W L, Lee K and Dahlburg R B 2006 *Phys. Plasmas* 13 032101
[34] Gentle K W, Liao K, Lee K and Rowan W L 2010 *Plasma Sci. Technol.* 12 391
[35] Toufen D L, Guimarães-Filho Z O, Caldas I L, Marcus F A and Gentle K W 2012 *Phys. Plasmas* 19 012307
[36] Toufen D L, Guimarães-Filho Z O, Caldas I L, Szezch J D, Lopes S, Viana R L and Gentle K W 2013 *Phys. Plasmas* 20 022310
[37] Toufen D L, Pereira F A C, Guimarães-Filho Z O, Caldas I L and Gentle K W 2014 *Phys. Plasmas* 21 122302
[38] Devynck P, Antar G, Wang G, Garbet X, Gunn J and Pascal J Y 2000 *Plasma Phys. Control. Fusion* 42 327
[39] Garcia O E et al *Nucl. Fusion* 47 667
[40] Levinson T, Beall J M, Powers E J and Bengtson R D 1984 *Nucl. Fusion* 24 527